Engineering Research
Express

INCLUSIVE PUBLISHING
TRUSTED SCIENCE

PURPOSE-LED
PUBLISHING™

PAPER

Decoupled optimization of a curved-beam compliant constant force mechanism

To cite this article: Yinong Liu *et al* 2026 *Eng. Res. Express* **8** 095515

View the article online for updates and enhancements.

You may also like

- Design and testing of a monolithic compliant constant force mechanism
Pietro Bilancia and Giovanni Berselli
- Intelligent optimization of compliant constant-force mechanism support extending work stroke
Xiao Zhang, Shuaishuai Lu, Yan Liu et al.
- Development of distributed compliant mechanism for two distinct applications: displacement amplifying and object holding mechanism
Sachin R Kandharkar, Sujit S Pardeshi, Rohan Soman et al.

This content was downloaded from IP address 134.74.20.15 on 02/06/2026 at 04:15

Engineering Research Express

Check for updates

RECEIVED
12 December 2025

REVISED
14 March 2026

ACCEPTED FOR PUBLICATION
15 April 2026

PUBLISHED
6 May 2026

PAPER

Decoupled optimization of a curved-beam compliant constant force mechanism

Yinong Liu[1], Hui Jiang[2], Zhijian He[3], Bo Wang[4], Jin Zhao[1] and Guangwei Wang[1,*]

[1] School of Mechanical Engineering, Guizhou University, Guiyang, People's Republic of China
[2] School of Intelligent Transportation and Engineering, Guangzhou Maritime University, Guangzhou, People's Republic of China
[3] College of Big Data and Internet, Shenzhen Technology University, Shenzhen, People's Republic of China
[4] Department of Mechanical Engineering, The City College of New York, New York, NY, United States of America
[*] Author to whom any correspondence should be addressed.

E-mail: gwwang@gzu.edu.cn

Keywords: compliant constant-force mechanism, curved-beam mechanism, optimization method, nonlinear stiffness regulator

Abstract

This paper addresses the trade-off between constant-force stroke and stability in compliant constant-force mechanisms (CCFMs). We introduce a novel CCFM topology that utilizes a curved beam as a nonlinear positive-stiffness regulator to mitigate the stiffness mismatch inherent in conventional designs. The decoupled two-stage optimization methodology is further proposed to independently tune the stroke and force magnitude of CCFMs. The optimized design achieves a constant-force stroke of 3080 μm, representing a 90.1% enhancement over a baseline design, while maintaining force fluctuation below 5% for the target constant force. This design process is facilitated by a Kriging-assisted framework, which yields a 69.3% gain in computational efficiency relative to direct optimization approaches. Experimental validation on a 3D-printed prototype confirmed its performance, delivering a 5.3 N constant force over a 3264 μm stroke. These results demonstrate that the synergistic use of the proposed topology and optimization strategy offers a robust pathway toward high-performance CCFMs for safe and reliable manipulation.

1. Introduction

Precision micromanipulation systems have seen substantial advancements in recent decades, enabling critical applications in aerospace [1], biomedical engineering [2], micro-manufacturing [3], and energy harvesting [4]. In such scenarios, the manipulated objects are frequently delicate, necessitating precise regulation of contact forces to prevent object damage and ensure operational repeatability [5, 6].

Conventional force control paradigms typically rely on active systems, coupling advanced sensing with sophisticated control algorithms [7]. While numerous advanced force sensors and control algorithms have been developed [8–10], these solutions inevitably increase system complexity, cost, and energy consumption, often at the expense of reliability [11]. Furthermore, miniaturization requirements impose additional integration challenges [12, 13]. In contrast, compliant constant-force mechanisms (CCFMs), whose ideal characteristic is depicted in figure 1, offer a compelling passive alternative. Benefiting from their monolithic construction, CCFMs eliminate assembly errors and friction [14]. By embedding force control directly into their structure, they also obviate the need for external feedback loops, thereby simplifying system design [15, 16].

The most common CCFM architecture operates on the stiffness-combination principle, where a negative-stiffness element is connected in parallel with a positive-stiffness element [12, 17]. For instance, Liu designed a passive compliant constant-force gripper employing serially connected drive and constant-force modules, with the latter operating on the stiffness-combination principle [18]. Wang developed a flexure-based constant-force XY precision positioning stage integrating bistable beams and positive-stiffness leaf flexures to achieve near-zero stiffness [19]. However, the performance of these mechanisms is fundamentally constrained by the inherent stiffness mismatch between their constituent elements. The negative stiffness is typically generated by inducing buckling in slender beams, an inherently

© 2026 IOP Publishing Ltd. All rights, including for text and data mining, AI training, and similar technologies, are reserved.

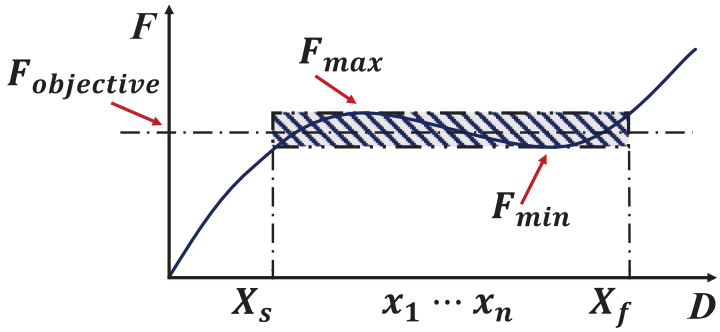

Figure 1. Idealized force–displacement characteristic of CCFM.

abrupt event characterized by sharp changes in the force–displacement (F–D) curve. Pairing this volatile negative-stiffness element with a conventional, often linear, positive-stiffness element makes stable stiffness cancellation over a wide range challenging to achieve. This intrinsic mismatch compromises the constant-force stroke and deteriorates force stability, creating a critical bottleneck for high-performance applications.

To address this challenge, researchers have explored various topologies. While some have focused on complex negative-stiffness configurations, another promising yet underexplored avenue is to redesign the positive-stiffness element. Incorporating curved beams, for instance, has shown potential for more diverse mechanical behaviors [20–22]. Pham utilized curved beams to create bistable mechanisms for overload protection [23]. Zhang proposed a quasi-constant force mechanism based on curved beams with a large range of constant force outputs to address force-sensitive manipulation [24]. Miao developed a CCFM based on curved beams to address the challenge of low-damage fruit picking for robotic harvesters [25]. Despite these advances, the systematic treatment of the curved beam as a nonlinear positive-stiffness regulator, specifically tailored to counterbalance the highly nonlinear buckling behavior, remains an underexplored area.

Furthermore, even with an improved mechanical topology, the design process for CCFMs remains a significant hurdle due to the complex, large-deformation mechanics involved. This complexity underscores the need for systematic optimization methods. Lan proposed a numerical method based on intrinsic functions and the generalized multiple shooting method for compliant mechanism shape design and optimization [26]. Chen subsequently applied this method to design a series of CCFMs [27, 28]. Wu optimized the structural parameters of a 1-DOF compliant platform using a multi-objective genetic algorithm (MOGA) [29]. Liu proposed a topology optimization method, leading to the development of a novel constant-force compliant finger [30]. Tong proposed an automatic optimization method for CCFMs based on finite element analysis (FEA) and experimentally validated the performance of the designed mechanism [31]. Despite these advancements, such methods typically treat the design as a fully coupled multi-objective problem, forcing a direct trade-off between the target force magnitude and the constant-force stroke. Consequently, the optimization process often converges to solutions where the desired force value is achieved at the expense of a compromised stroke, or vice-versa.

This paper overcomes these dual limitations by introducing two primary contributions. First, we propose a novel CCFM topology in which an engineered curved beam serves as a nonlinear positive-stiffness regulator. Unlike prior curved-beam (CB) designs that focused on standalone force outputs, the proposed topology is specifically tailored to counterbalance the abrupt buckling behavior of the negative-stiffness element, enabling stable stiffness cancellation over a wide displacement range. Second, informed by the finding that the out-of-plane width acts as a pure force scalar while other geometric parameters govern the curve shape, we develop a decoupled two-stage optimization strategy that independently maximizes the constant-force stroke and subsequently tunes the force magnitude, avoiding the coupled trade-off inherent in existing methods. The efficacy of both contributions is validated through FEA, experimental testing of a 3D-printed prototype, and a practical low-damage gripping demonstration.

The remainder of this paper is organized as follows: section 2 presents the mechanism design and analytical modeling. Section 3 details the parametric sensitivity analysis and formulates the optimization objectives. The proposed optimization methodology is presented in section 4. In section 5, the prototype is experimentally validated, and a physical gripping experiment is performed. Finally, section 6 concludes this paper.

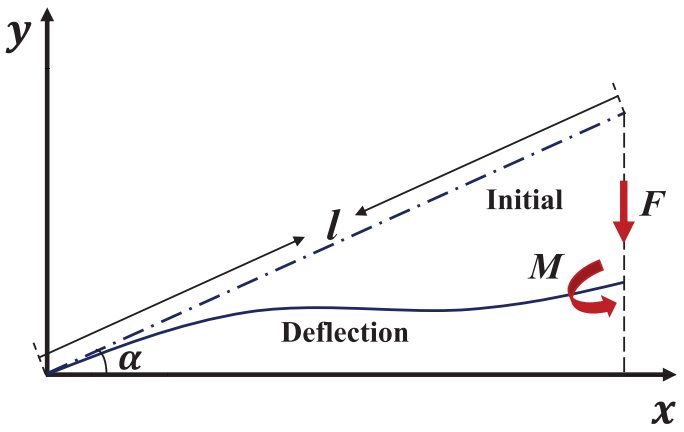

Figure 2. Force-deformation behavior of a bistable beam.

2. Mechanism design and modeling

The design of the proposed CCFM is founded on the stiffness combination principle, where a positive-stiffness element and a negative-stiffness element are connected in parallel. The total stiffness and force of the mechanism are the superposition of its constituent elements, aiming to achieve a near-zero total stiffness over a desired displacement range. This is achieved when the positive stiffness effectively cancels the negative stiffness.

$$K_{\text{total}} = K_{\text{positive}} + K_{\text{negative}} \tag{1}$$

$$F_{\text{total}} = F_{\text{positive}} + F_{\text{negative}} \tag{2}$$

where K is stiffness and F is force output. While the principle is straightforward, the performance of the CCFM is highly dependent on the nonlinear characteristics of these elements.

2.1. Design of the negative-stiffness mechanism

The negative-stiffness characteristic is generated using a classic pre-buckled bistable beam, as depicted in figure 2. This element is widely employed for its predictable and highly nonlinear *F–D* behavior. To capture this behavior under large deflections, we employ the well-established elliptic integral model, derived from Euler–Bernoulli beam theory. As the complete derivation is detailed extensively in prior work [19, 32], only the final governing equations are presented. These equations relate the beam's end coordinates (x_c, y_c) to its geometric parameters:

$$\frac{y_c}{l} = -\frac{1}{R}\{2\sin\alpha\,(\Delta E - \Delta F) + 2u\cos\alpha\,\Delta C\} \tag{3}$$

$$\frac{x_c}{l} = -\frac{1}{R}\{2\cos\alpha\,(\Delta E - \Delta F) + 2u\sin\alpha\,\Delta C\} \tag{4}$$

where $\Delta E = E(u, v_2) - E(u, v_1)$, $\Delta F = F(u, v_2) - F(u, v_1)$, and $\Delta C = \cos v_1 - \cos v_2$ are used for conciseness. The parameters l and α represent the beam length and initial inclination angle, respectively, while $F(u, v)$ and $E(u, v)$ are the incomplete elliptic integrals of the first and second kind.

2.2. Design of the positive-stiffness mechanism

The selection of an appropriate positive-stiffness element is pivotal for overcoming the inherent stiffness mismatch in conventional CCFMs. While straight beams are common, they exhibit a strong stress-stiffening effect under large deflections, leading to a rapid increase in stiffness that is difficult to counteract [31, 33, 34]. To address this, we introduce a curved beam, composed of two tangentially connected quarter-circles, that acts as a nonlinear positive-stiffness regulator.

To quantitatively demonstrate the superiority of this design, we performed a comparative FEA against a conventional fixed-guided straight beam. To ensure a fair comparison within a similar spatial envelope, the straight beam's length was set equal to the curved beam's diameter. The structural parameters are listed in table 1, and both components were modeled using ABS plastic.

Table 1. Structural parameters for comparative FEA of positive-stiffness elements.

	Parameter	Value	Unit
Straight beam	length	40	mm
	in-plane thickness	1	mm
	out-of-plane width	4	mm
Curved beam	radius	20	mm
	in-plane thickness	1	mm
	out-of-plane width	4	mm

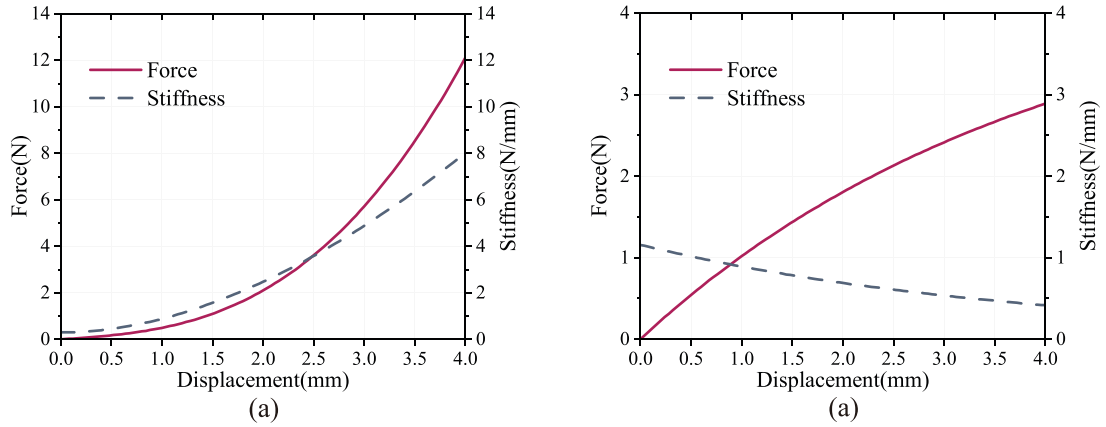

Figure 3. FEA of positive-stiffness elements. (a) Force–displacement response and stiffness of a straight beam, showing significant stress-stiffening. (b) The proposed curved beam exhibits a gradually varying stiffness over a large deformation.

The results, shown in figure 3, reveal a stark contrast in their mechanical behavior. The straight beam exhibits significant stiffening: its stiffness increases dramatically from 0.3 N mm^{-1} to 7.95 N mm^{-1} over a 4 mm deformation (figure 3(a)). This sharp rise is characteristic of the stress-stiffening effect, rendering it incompatible with a buckling-based negative-stiffness element. In contrast, the proposed curved beam maintains remarkable stiffness stability over a 4 mm deformation, with its stiffness varying gently from 0.42 N mm^{-1} to 1.15 N mm^{-1} (figure 3(b)). This desirable behavior arises because the curved geometry transforms the applied displacement primarily into bending deformation, mitigating the tensile stresses that cause stiffening in straight beams.

This analysis confirms that the curved beam, with its gradually varying nonlinear positive stiffness, provides a much more stable and compatible counterpart to the volatile negative-stiffness element, making it the superior choice for designing a large-stroke CCFM.

2.3. Integrated mechanism and baseline performance

The proposed CB-CCFM is constructed by connecting the bistable beams and the curved beams in parallel, as shown in figure 4. To establish a performance baseline for subsequent optimization, an initial proof-of-concept design was created with the structural parameters listed in table 2.

An FEA model incorporating large deflection and material nonlinearities was used to evaluate this baseline design. While the simulation confirms the constant-force principle, the performance is suboptimal for practical applications, exhibiting an arbitrary constant force value and a limited stroke. This highlights a critical challenge: achieving a user-defined target force while simultaneously maximizing the constant-force stroke cannot be reliably accomplished through manual trial-and-error [31, 32]. A systematic optimization methodology is therefore essential to unlock the mechanism's full potential, as detailed in the following sections.

3. Parametric analysis and optimization objectives

To develop an effective optimization strategy, it is crucial to first understand how each geometric parameter influences the *F–D* characteristics of the CB-CCFM. This section presents a parametric sensitivity

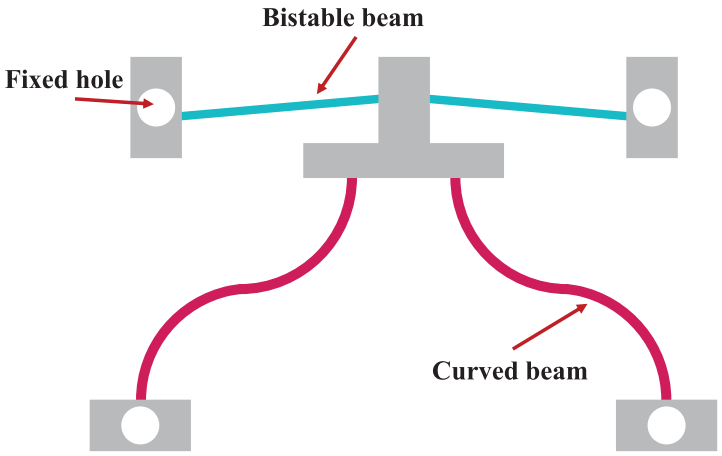

Figure 4. Schematic of the proposed CB-CCFM.

Table 2. Initial structural parameters of the baseline CB-CCFM.

	Parameter	Value	Unit
Bistable beam	Angle (θ)	5.1	Degree
	Length (l)	29	mm
	In-plane thickness (t_b)	1.2	mm
	Out-of-plane width (w)	4	mm
Curved beam	Radius (r)	20	mm
	In-plane thickness (t_c)	1.3	mm
	Out-of-plane width (w)	4	mm

analysis aimed at classifying the design variables into distinct functional groups. This classification forms the foundation for our proposed decoupled optimization methodology, allowing us to reformulate the complex design problem into two sequential, more tractable sub-problems.

3.1. Parametric sensitivity analysis

A sensitivity analysis was performed by systematically varying one geometric parameter at a time from its baseline value in table 2, with the results obtained via FEA shown in figure 5. The analysis reveals that the design variables can be classified into two functionally distinct groups.

The bistable beam's angle θ, length l, and in-plane thickness t_b, along with the curved beam's radius r and in-plane thickness t_c, are identified as shape-controlling parameters. As shown in figures 5(a)–(e), altering any of these variables significantly changes the nonlinear shape of the F–D curve. These parameters collectively determine the critical points of the curve, such as the initial stiffness, the peak force, the negative stiffness slope, and the final stiffening behavior. Consequently, they are the primary determinants of the constant-force stroke and force stability. Conversely, the out-of-plane width w functions explicitly as a scale-controlling parameter. Figure 5(f) demonstrates that varying w acts as a nearly linear scalar on the force magnitude. While the absolute force values change proportionally with w, the normalized shape of the curve and constant-force stroke remain virtually unchanged.

Hence, this result enables us to decouple the optimization problem, moving beyond the inherent limitations of traditional approaches.

3.2. Formulation of optimization problem

CCFMs aim to produce a nearly flat F–D characteristic curve. However, manufacturing imperfections, material nonlinearity, and dynamic coupling effects introduce deviations that manifest as force oscillations around the target value F_{obj}, as shown in figure 1. To improve the practical significance of CCFMs, the F–D curve should also be tunable to accommodate diverse operational requirements. Informed by the preceding sensitivity analysis, we reformulate this conventional multi-objective design challenge as a decoupled, two-stage optimization problem.

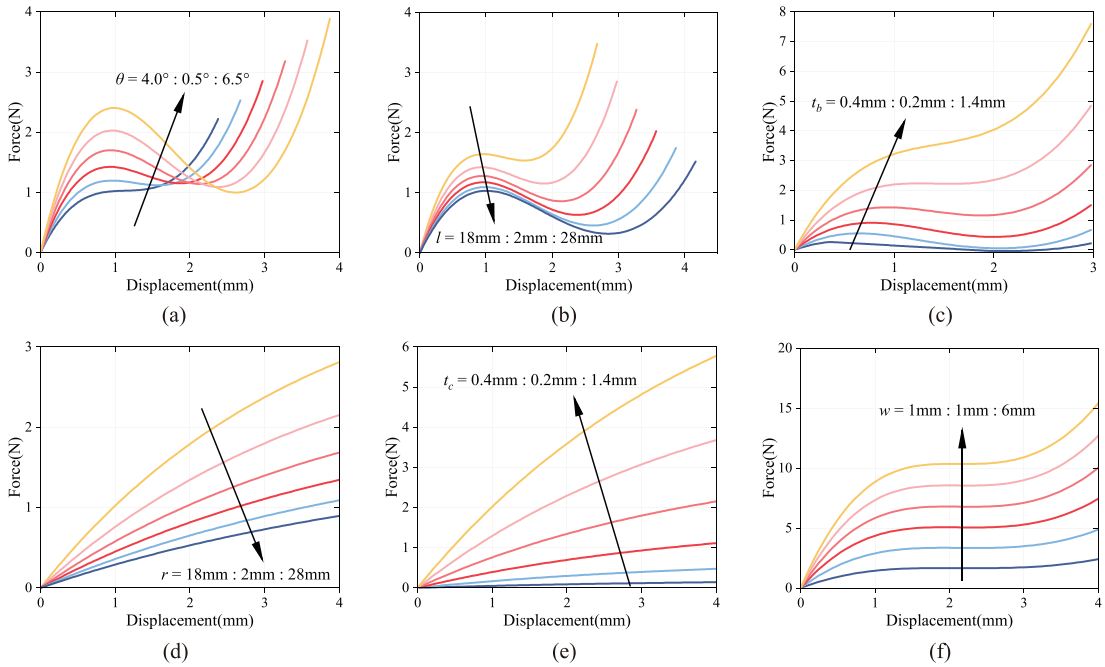

Figure 5. Parameter sensitivity analysis results when changing the (a) bistable beam inclined angle, (b) bistable beam length, (c) bistable beam in-plane thickness, (d) curved beam radius, (e) curved beam in-plane thickness, (f) mechanism out-of-plane width.

3.2.1. Geometric parameter optimization

The primary goal of this stage is to determine the optimal geometric shape of the mechanism to maximize its kinematic performance, independent of the absolute force magnitude. The objectives are to maximize the constant-force stroke S and minimize the force fluctuation ΔF, a measure of stability. The constant-force region $[X_s, X_f]$ is defined based on a $\pm 5\%$ tolerance band around the mean force μ within the stroke, as illustrated in figure 1. Specifically, X_s is the displacement at which the force first enters the band $[0.95\mu, 1.05\mu]$, and X_f is the displacement at which the force last leaves this band. The multi-objective optimization problem for this stage is formulated as:

$$\begin{aligned} &\text{Maximize:} \quad S(X) = X_f - X_s \\ &\text{Minimize:} \quad \Delta F(X) = \frac{1}{N}\sum_{i=1}^{N}(F_i - \mu(X))^2 \end{aligned} \tag{5}$$

where $X = [\theta, l, t_b, r, t_c]$ is the vector of shape-controlling parameters, $\mu(X)$ is the mean force over the stroke, and N is the number of sample points.

3.2.2. Force magnitude tuning

After the optimal shape parameter vector X^* is determined in the previous stage, the second stage aims to tune the mechanism to a user-defined target force F_{obj}, without compromising the already optimized stroke and stability. This is achieved by adjusting the scale-controlling parameter w. The objective is formulated as:

$$\text{Minimize: } |\mu(X^*, w) - F_{\text{obj}}|. \tag{6}$$

By structuring the problem in this manner, we transform a complex, coupled multi-objective challenge into two simpler, sequential tasks. This decoupled framework provides a more robust and efficient path to achieving high-performance CCFMs tailored to specific application requirements. The detailed implementation of this strategy is presented in the following section.

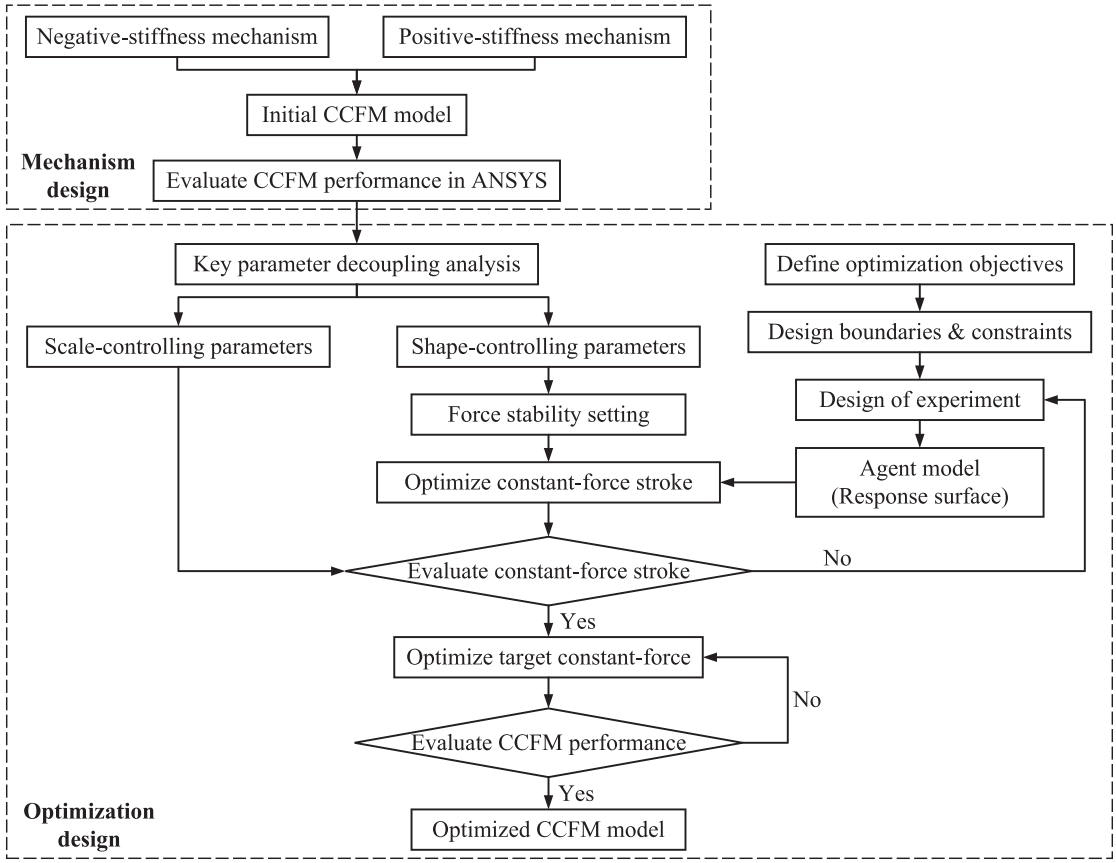

Figure 6. Flowchart of the proposed two-stage optimization procedure.

4. Optimization method and results

4.1. Optimization framework

To efficiently solve the decoupled optimization problem, we developed a two-stage optimization framework, illustrated in figure 6. Directly coupling FEA with a MOGA is computationally prohibitive. Therefore, our framework first constructs a Kriging surrogate model based on a limited number of FEA simulations. This surrogate model provides a near-instantaneous approximation of the mechanism's *F–D* response, enabling the MOGA to explore the vast design space efficiently.

4.2. Stage 1: geometric parameter optimization

The initial stage focuses on optimizing the set of shape-controlling parameters, $X = [\theta, l, t_b, r, t_c]$, to maximize the constant-force stroke while ensuring force stability and structural integrity. To construct a high-quality response surface based on the Kriging model, a training dataset was generated across the design space of the shape-controlling parameters to ensure the model's predictive accuracy while maintaining a manageable computational budget for the initial FEA simulations.

The MOGA was then deployed to search for the Pareto-optimal frontier on the resulting Kriging surface, with the primary objectives being the maximization of the constant-force stroke and the minimization of normalized force fluctuation. While these kinematic metrics drove the optimization, the final selection of a candidate design from the Pareto front was further guided by auxiliary engineering criteria to ensure structural robustness. Specifically, solutions exhibiting a lower equivalent stress maximum and a higher total deformation average were deemed preferable, as they indicate superior material utilization and deformation capacity.

4.3. Stage 2: scale tuning

With the optimal shape parameters X^* established, the second stage is a straightforward single-variable problem: tuning the scale-controlling parameter, the out-of-plane width w, to match the user-defined target force F_{obj}. The optimal width w^* is found by solving the simple minimization problem.

Note that in more complex cases involving two or more parameters, the response surface model can still be employed to quickly identify structural parameter values that achieve the target constant force.

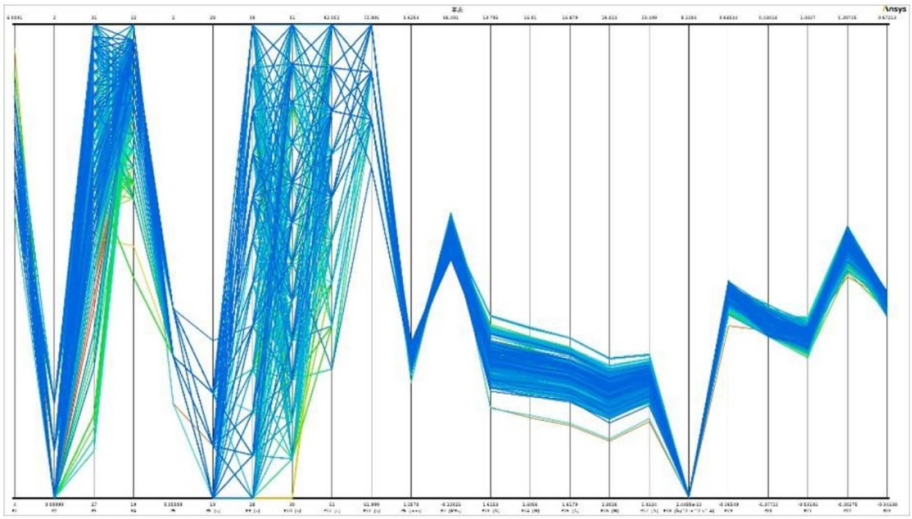

Figure 7. Schematic of sampling points during the optimization process.

Table 3. Comparison of initial and optimized structural parameters of the CB-CCFM.

	Parameter	Initial	Optimized	Change	Unit
Bistable beam	Angle (θ)	5.1	5.8	+13.7%	Degree
	Length (l)	29	34	+17.2%	mm
	In-plane thickness (t_b)	1.2	1.1	−8.3%	mm
	Out-of-plane width (w)	4	3	−25.0%	mm
Curved beam	Radius (r)	20	20.9	+4.5%	mm
	In-plane thickness (t_c)	1.3	1.4	+7.7%	mm
	Out-of-plane width (w)	4	3	−25.0%	mm

By effectively decoupling force tuning from geometric parameter optimization, this step overcomes the inherent limitations of conventional coupled design methods.

The design variables for the entire optimization process were bounded by the following constraints:

$$\text{s.t.}: \begin{cases} \theta \in [4:0.1:6] \ \text{deg} \\ l \in [27:0.1:36] \ \text{mm} \\ t_b, t_c \in [1:0.1:2] \ \text{mm} \\ r \in [19:0.1:22] \ \text{mm} \\ w \in [1:1:6] \ \text{mm}. \end{cases} \tag{7}$$

4.4. Optimization results

The optimization was performed on a workstation with an Intel i7-9700KF CPU @ 3.60 GHz and 16 GB RAM. In stage 1, the MOGA converged to an optimal set of shape parameters after approximately 35 000 evaluations on the fast-running surrogate model. In stage 2, the optimal width was determined nearly instantaneously. Figure 7 is a schematic of the sampling points during the optimization process. The final set of optimized structural parameters is listed in table 3.

The resulting performance, compared against the baseline design in figure 8, demonstrates the efficacy of the proposed framework. The optimized design achieves the target constant force of 5.3 N over a 3080 μm stroke (from 1265 to 4345 μm), with force fluctuations maintained within the 5% target. This represents a substantial 90.1% enhancement in constant-force stroke over the 1600 μm stroke of the baseline design. Furthermore, compared to a conventional straight-beam CCFM optimized using a comparable approach [31], the CB topology achieves a significantly larger stroke gain (90.1% vs 20.9%) with a tighter force fluctuation criterion, underscoring the critical role of the CB geometry in overcoming the stress-stiffening limitation. In addition, the Kriging-assisted surrogate framework reduces computational cost by an estimated 69.3% compared to direct FEA-based optimization, enabling efficient exploration of the design space.

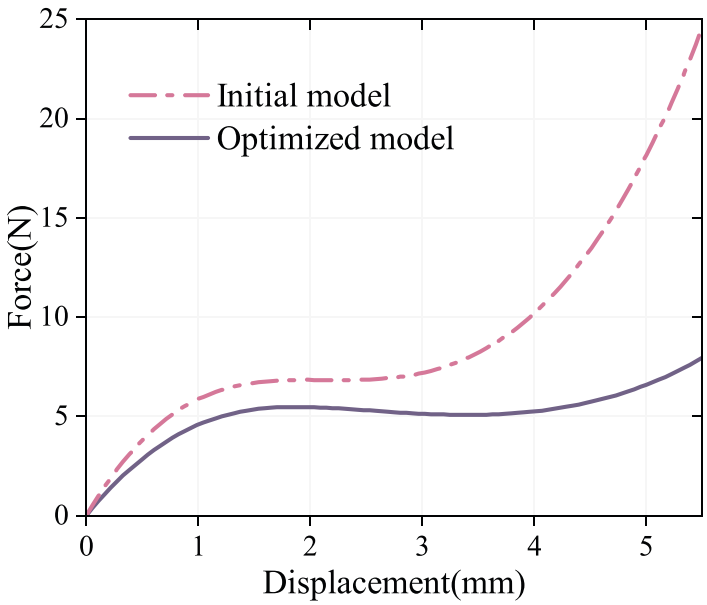

Figure 8. Comparison of the baseline and optimized models.

Table 4. Mechanical properties of ABS plastic.

Property	Value	Unit
Density	1040	$kg\,m^{-3}$
Young's modulus	2.39	GPa
Poisson's ratio	0.399	/
Bulk modulus	3.944	GPa
Shear modulus	0.854	GPa
Tensile yield strength	41.4	MPa
Tensile ultimate strength	44.3	MPa

5. Experimental validation

5.1. Prototype fabrication and experimental setup

To validate the performance of the optimized CB-CCFM, multiple physical prototypes were fabricated from ABS plastic using fused deposition modeling (FDM) 3D printing. To ensure high fidelity between the simulation model and the physical prototype, the material properties used in the FEA and optimization stages represent the effective properties characterized from 3D-printed specimens, as listed in table 4.

The prototype, shown in figure 9, was integrated with a rigid outer frame to facilitate mounting without affecting the deformation of its compliant members. The experimental setup was designed for high-precision characterization. A voice coil motor (model: VCAR-0044-0249-00A) with an integrated linear encoder provided precisely controlled input displacement, which was managed by a real-time controller (model: NI-cRIO 9047). A miniature force sensor (model: FUTEK LSB201), mounted at the output stage, measured the reaction force. Data from the sensor and encoder were synchronized and acquired by a host PC for analysis. The force sensor has a combined nonlinearity and hysteresis of $\pm 0.1\%$ of rated output, and the linear encoder provides micrometer-level displacement resolution, ensuring that measurement uncertainty is negligible at the magnitude of 5.3 N.

5.2. Constant-force experimental results and analysis

The prototype was subjected to a quasi-static displacement-controlled test. To ensure repeatability and minimize random errors, a representative prototype was selected and tested five times to obtain averaged results. Figure 10 compares the experimental *F–D* curve with the results from the FEA simulation.

The experimental results show a constant force output of 5.3 N over a 3264 μm stroke (from 2077 to 5341 μm), with force fluctuations well within the 5% target defined during optimization. This result is in excellent agreement with the design objectives.

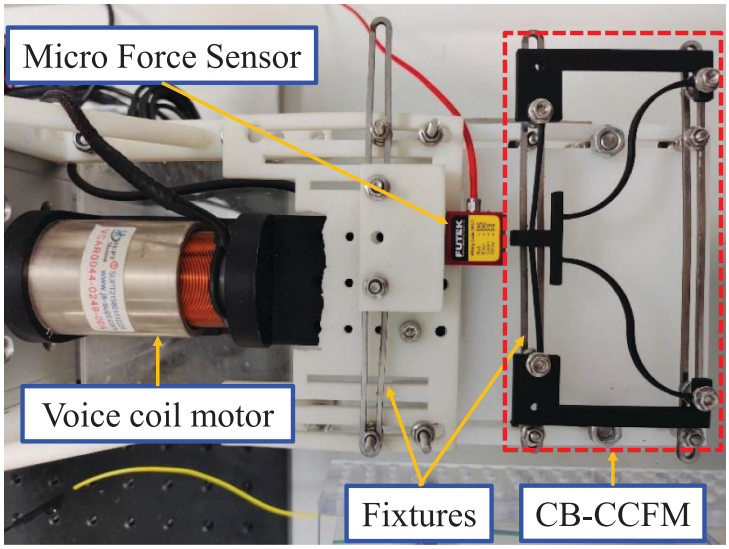

Figure 9. Experimental setup for the proposed CB-CCFM prototype.

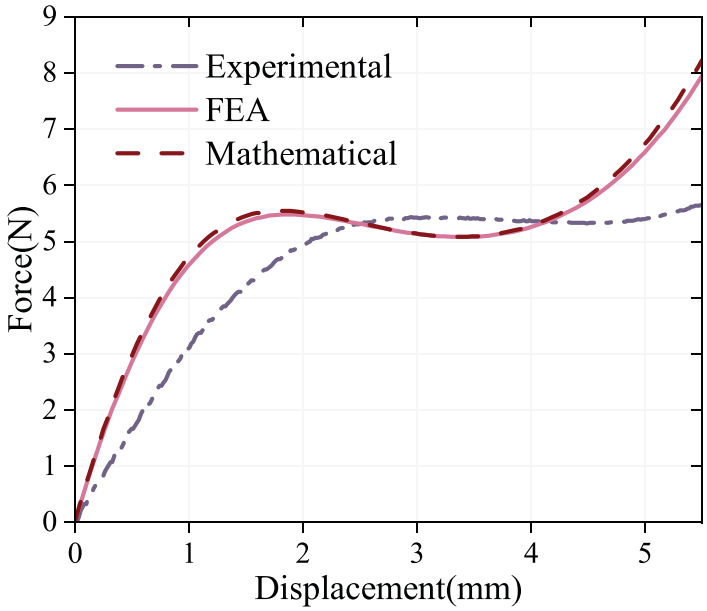

Figure 10. Comparison of force–displacement characteristic curves.

Notably, the magnitude and accuracy of the constant force in the experimental results are consistent with the simulation results, while the constant force stroke has increased by approximately 5.6%, and the constant force interval as a whole is shifted backward.

This shift can be attributed to the inherent characteristics of the FDM fabrication process. Minor geometric deviations and anisotropy in the printed material can slightly alter the prestress conditions of the bistable beams, thus shifting the precise displacement at which buckling is initiated. Furthermore, the constant-force characteristics of the prototype can be altered by FDM process imperfections, such as internal voids resulting from non-uniform cooling and geometric inaccuracies at critical boundary connections. Nevertheless, the fact that the mechanism's core constant-force behavior is robustly maintained despite these real-world imperfections strongly validates the proposed design and the optimization methodology.

5.3. Application demonstration: low-damage gripping

To demonstrate the practical utility and passive force-limiting capability of the CB-CCFM, a delicate object gripping experiment was conducted using a blueberry, a fruit known to be highly susceptible to

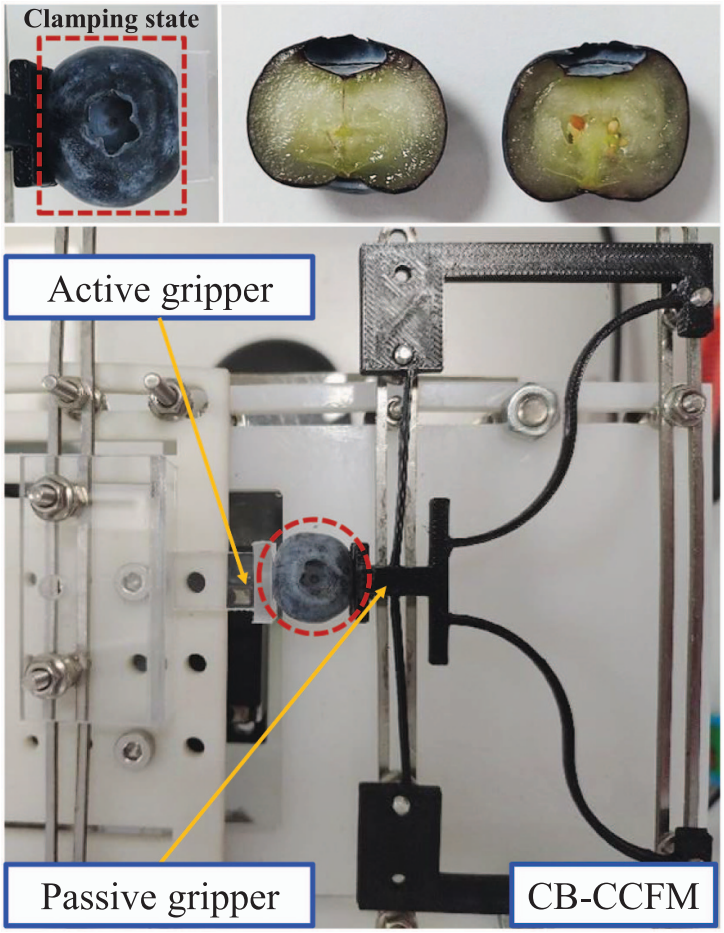

Figure 11. Demonstration of low-damage gripping capability.

damage from excessive force [35]. The mechanism was actuated to grip the blueberry (figure 11), passively limiting the contact force due to its inherent constant-force characteristic.

To assess for internal damage, the gripped blueberry was subsequently sectioned and compared to an untouched control sample, as shown in figure 11. The blueberry on the right is being gripped, and the blueberry on the left is a normal one. Visual inspection revealed no discernible internal bruising, thereby attesting to the mechanism's capability for low-damage manipulation (gripped blueberry (right) and). This experiment highlights the significant potential of the proposed CB-CCFM for applications requiring the safe and reliable manipulation of delicate biological samples, micro-components, or other force-sensitive objects.

6. Conclusion

This paper has introduced and experimentally validated a large-stroke CCFM, addressing the fundamental trade-off between constant-force range and stability in conventional designs. The curved beam is utilized as a nonlinear positive-stiffness regulator to mitigate abrupt buckling, and a decoupled two-stage optimization methodology to enable independent tuning of the mechanism's kinematic performance and force magnitude. The resulting optimized design achieved a target force of 5.3 N over a 3080 μm stroke with less than 5% fluctuation. These performance metrics were successfully validated by a 3D-printed prototype, which delivered the same constant force over a 3264 μm stroke and confirmed its utility in a practical low-damage gripping application. Beyond this specific mechanism, the proposed decoupled optimization framework offers a generalizable design paradigm for a broader class of compliant systems where competing performance objectives hinder traditional design approaches. As the curved beam's decreasing-stiffness behavior is geometry-driven, the concept readily extends to higher-stiffness materials with appropriate parameter re-optimization. Future work will leverage this validated framework to

develop integrated compliant constant-force grippers, aiming to further advance force control solutions for precision micromanipulation.

Data availability statement

All data that support the findings of this study are included within the article (and any supplementary files).

Funding

This research was funded by the National Natural Science Foundation of China (Grant 52 265 070), Zhuhai Industry-Academia Cooperation R&D Project (Grant 23 200 0400 2732).

ORCID iDs

Bo Wang 0000-0001-6047-1400
Guangwei Wang 0000-0002-1794-0619

References

[1] Bai R, Yang N, Li B and Chen G 2024 Nonlinear strain energy formulation of spatially deflected strip flexures *Mech. Mach. Theory* **195** 105594
[2] Thomas T L, Venkiteswaran V K, Ananthasuresh G and Misra S 2021 Surgical applications of compliant mechanisms: a review *J. Mech. Robot.* **13** 020801
[3] Rakotondrabe M, Ivan I A, Khadraoui S, Lutz P and Chaillet N 2014 Simultaneous displacement/force self-sensing in piezoelectric actuators and applications to robust control *IEEE/ASME Trans. Mechatronics* **20** 519–31
[4] Liu H, Zhong J, Lee C, Lee S-W and Lin L 2018 A comprehensive review on piezoelectric energy harvesting technology: materials, mechanisms and applications *Appl. Phys. Rev.* **5** 041306
[5] Li X, Liu Y, Ge L and Zhang Z 2024 A large-stroke reluctance-actuated nanopositioner: compliant compensator for enhanced linearity and precision motion control *IEEE/ASME Trans. Mechatronics* **29** 2947–55
[6] Ling J, Ye T, Feng Z, Zhu Y, Li Y and Xiao X 2022 A survey on synthesis of compliant constant force/torque mechanisms *Mech. Mach. Theory* **176** 104970
[7] Wei Y and Xu Q 2018 A survey of force-assisted robotic cell microinjection technologies *IEEE Trans. Autom. Sci. Eng.* **16** 931–45
[8] Wei Y and Xu Q 2015 An overview of micro-force sensing techniques *Sens. Actuators A* **234** 359–74
[9] Mauser K and Hasse A 2020 How to prestress compliant mechanisms for a targeted stiffness adjustment *Smart Mater. Struct.* **29** 085021
[10] Xu H, Zhang X, Zang H, Lai J, Yuan L and Wang R 2024 An SMA-based compliant adjustable constant force gripper for microassembly *Int. J. Mech. Sci.* **278** 109430
[11] Xu Q 2017 Design of a constant-force microgripper mechanism for biological micromanipulation *2017 IEEE 12th Int. Conf. on Nano/Micro Engineered and Molecular Systems (NEMS)* (IEEE) pp 418–21
[12] Wang P and Xu Q 2018 Design and modeling of constant-force mechanisms: a survey *Mech. Mach. Theory* **119** 1–21
[13] Bilancia P and Berselli G 2020 Design and testing of a monolithic compliant constant force mechanism *Smart Mater. Struct.* **29** 044001
[14] Banerjee P, Balaji P, Leblouba M and Murugan S 2025 Displacement and force transmissibility of a quasi-zero-stiffness-based compliant metamaterial structure *Smart Mater. Struct.* **34** 035009
[15] Wu K, Zheng G, Chen G and Awtar S 2024 A body-frame beam constraint model *Mech. Mach. Theory* **192** 105517
[16] Shao Y, Wang Z, Sun Y, Shi D, Feng Y, Liu F, Ding X and Zhang W 2025 Design of an adjustable constant force mechanism based on integrated magnet-beam structures and an adjustable lever mechanism *Mech. Mach. Theory* **209** 105997
[17] Wang P, Nan Z and Xu Q 2018 Design of a new XYZ parallel stage with near constant driving force *2018 3rd Int. Conf. on Advanced Robotics and Mechatronics (ICARM)* (IEEE) pp 177–82
[18] Liu Y, Zhang Y and Xu Q 2016 Design and control of a novel compliant constant-force gripper based on buckled fixed-guided beams *IEEE/ASME Trans. Mechatronics* **22** 476–86
[19] Wang P and Xu Q 2017 Design of a flexure-based constant-force XY precision positioning stage *Mech. Mach. Theory* **108** 1–13
[20] Chen Q, Wen Q, Zhang X, Yang Y and Xiao S 2024 Buckling-induced instability in topology optimization of compliant constant-force mechanisms *Mech. Mach. Theory* **191** 105475
[21] Wang W, Jin M, Li Z, Qu M and Xu X 2024 Two prbms of Euler spiral segments and their chained models for analyzing general curved beams in compliant mechanisms *Mech. Mach. Theory* **204** 105838
[22] Gan J, Xu H, Zhang X and Ding H 2022 Design of a compliant adjustable constant-force gripper based on circular beams *Mech. Mach. Theory* **173** 104843
[23] Pham H-T and Wang D-A 2011 A constant-force bistable mechanism for force regulation and overload protection *Mech. Mach. Theory* **46** 899–909
[24] Zhang Q, Yan P and Wang H 2022 A curved-beam based quasi-constant force mechanism supporting large range and force-sensitive robotic manipulation *Mech. Mach. Theory* **172** 104799
[25] Miao Y and Zheng J 2020 Optimization design of compliant constant-force mechanism for apple picking actuator *Comput. Electron. Agric.* **170** 105232

[26] Lan C-C and Cheng Y-J 2008 Distributed shape optimization of compliant mechanisms using intrinsic functions *J. Mech. Des.* **130** 072304
[27] Chen Y-H and Lan C-C 2012 An adjustable constant-force mechanism for adaptive end-effector operations *J. Mech. Des.* **134** 031005
[28] Chen Y-H and Lan C-C 2012 Design of a constant-force snap-fit mechanism for minimal mating uncertainty *Mech. Mach. Theory* **55** 34–50
[29] Wu Z and Xu Q 2018 Design, fabrication and testing of a new compact piezo-driven flexure stage for vertical micro/nanopositioning *IEEE Trans. Autom. Sci. Eng.* **16** 908–18
[30] Liu C-H, Chung F-M and Ho Y-P 2021 Topology optimization for design of a 3D-printed constant-force compliant finger *IEEE/ASME Trans. Mechatronics* **26** 1828–36
[31] Tong Z, Zhang X and Wang G 2023 Automatic optimization for compliant constant force mechanisms *Actuators* **12** 61
[32] Liu Y, He J and Wang G 2024 Efficient automatic optimization for compliant constant force mechanisms based on response surface method *2024 Int. Conf. on Advanced Robotics and Mechatronics (ICARM)* (IEEE) pp 946–51
[33] Wang P and Xu Q 2016 Design of a compact compliant constant-force XY precision positioning stage *2016 12th IEEE/ASME Int. Conf. on Mechatronic and Embedded Systems and Applications (MESA)* (IEEE) pp 1–6
[34] Zhang X and Xu Q 2019 Design and testing of a novel 2-DOF compound constant-force parallel gripper *Precis. Eng.* **56** 53–61
[35] Hou J, Park B, Li C and Wang X 2024 A multiscale computation study on bruise susceptibility of blueberries from mechanical impact *Postharvest Biol. Technol.* **208** 112660